Atom-in-jellium equations of state in the high-energy-density regime

Damian C. Swift,[1,*] Thomas Lockard,[1] Richard G. Kraus,[1] Lorin X. Benedict,[1] Philip A. Sterne,[1] Mandy Bethkenhagen,[1,†] Sebastien Hamel,[1] and Bard I. Bennett[2]

[1]*Lawrence Livermore National Laboratory, 7000 East Avenue, Livermore, California 94551, USA*

[2]*Los Alamos National Laboratory, PO Box 1663, Los Alamos, New Mexico 87545, USA*

(Received 28 September 2018; published 28 June 2019)

Recent path-integral Monte Carlo and quantum molecular dynamics simulations have shown that computationally efficient average-atom models can predict thermodynamic states in warm dense matter to within a few percent. One such atom-in-jellium model has typically been used to predict the electron-thermal behavior only, although it was previously developed to predict the entire equation of state (EOS). We report completely atom-in-jellium EOS calculations for Be, Al, Si, Fe, and Mo, as elements representative of a range of atomic number and low-pressure electronic structure. Comparing the more recent method of pseudoatom molecular dynamics, atom-in-jellium results were similar: sometimes less accurate, sometimes more. All these techniques exhibited pronounced effects of electronic shell structure in the shock Hugoniot which are not captured by Thomas-Fermi based EOS. These results demonstrate the value of a hierarchical approach to EOS construction, using average-atom techniques with shell structure to populate a wide-range EOS surface efficiently, complemented by more rigorous three-dimensional multiatom calculations to validate and adjust the EOS.

DOI: 10.1103/PhysRevE.99.063210

I. INTRODUCTION

Accurate equations of state (EOS) are essential to understand stellar and planetary formation and evolution, astrophysical impacts, and engineering challenges such as the development of inertial confinement fusion energy sources and the design and interpretation of experiments involving high-energy density (HED) plasmas such as those using pulsed electrical discharges and laser ablation. Experiments to measure the properties of matter in these conditions are difficult and expensive, and wide-ranging EOS are needed even to design and interpret such experiments.

Widely used EOS such as those in the SESAME and LEOS libraries [1,2] are usually constructed by combining relatively simple semiempirical models valid over a limited range of states, such as Thomas-Fermi (TF) or Thomas-Fermi-Dirac (TFD) theory [3,4] for high compressions and temperatures, hard-sphere models of the liquid-vapor region [5], and measurements of the shock Hugoniot. Evolving experimental capabilities and more rigorous theoretical investigations of localized regions of the EOS have identified inaccuracies, driving efforts to construct improved EOS. However, the most rigorous techniques expected to be applicable for warm dense matter, path-integral Monte Carlo (PIMC) [6] and quantum molecular dynamics (QMD) [7], are computationally expensive and not currently practical for the direct generation of wide-ranging EOS or for materials of high atomic number Z.

The most rigorous theoretical techniques simulate the kinetic motion of an ensemble of atoms, where the distribution of the electrons is found with respect to the changing location of the ions using quantum mechanics [6,7]. Despite their rigor, calculations using these techniques are not necessarily accurate. Many-body quantum mechanics is based on approximations to address the problem of representing anticommuting fermion wave functions, the fixed-node approximation [8] in PIMC, and the local density approximation [9,10] to the exchange-correlation functional in QMD. Calculations using either technique are converged to a finite degree with respect to numerical parameters such as the series-sum representation of wave functions, the computation of wave functions at a finite set of points in space (real or reciprocal), and the size of the ensemble of atoms. The energy of the ensemble is determined from an average over a sufficient time interval, and the heat capacity can be found from the rate of change of energy with temperature. This procedure is computationally expensive, requiring $o(10^{15})$ or more floating-point operations per state, equivalent to hundreds of CPU hours per state for QMD and thousands of CPU hours for PIMC. It is typically deemed impractical to perform these simulations for matter around or below ambient density and above a few tens of electron volts using QMD.

Recent PIMC and QMD results have indicated that the simpler approach of calculating the electron states for a single atom in a spherical cavity within a uniform charge density of ions and electrons, representing the surrounding atoms, reproduces their more rigorous EOS [11,12]. This atom-in-jellium approach [13] was developed originally to give improved accuracy over Thomas-Fermi-based EOS near ambient conditions. It was used previously to predict the electron-thermal energy of matter at high temperatures and compressions [1,14], as an advance over the approximation of a uniform electron gas, as in TF and related approaches.

Other techniques are being developed as more advanced compromises between the accuracy of multiatom calculations

*dswift@llnl.gov

†Present address: Universität Rostock, 18051 Rostock, Germany.

and the efficiency of the jellium approach, such as orbital-free molecular dynamics [15] and pseudoatom molecular dynamics [16] (PAMD). PAMD is based on a higher-order representation of electronic states in the jellium and includes ionic structure self-consistently, deducing an effective interatomic potential which can then be used to perform molecular dynamics (MD) simulations. PAMD calculations of Be, Al, Si, and Fe produce similar states to PIMC and QMD [17]. PAMD requires much less computational effort than PIMC or QMD, but it still amounts to several tens of CPU hours per state, so the construction of a wide-ranging tabular EOS is a significant undertaking.

One advantage of these average-atom techniques over QMD is that calculations of a single atom are fast enough that all electrons can be treated explicitly under all circumstances. For computational efficiency in QMD simulations, the inner electrons are typically subsumed into a pseudopotential, which would ideally be fixed and universal over the full range of the EOS. In practice, for wide-range EOS, the pseudopotential must be changed or abandoned at states of very high density or temperature.

The atom-in-jellium theory was previously extended to predict frequencies of vibration for ions perturbed from equilibrium in the jellium, and hence the Debye temperature [18], which was assessed as being correct to within ∼15% for close-packed structures. The Debye model can be used to predict the ion-thermal free energy, so this development made it possible in principle to calculate the complete EOS from atom-in-jellium theory. However, this does not appear to have been done.

In the work reported here, we made some corrections to the previous jellium vibrations model, and calculated EOS to provide a broad comparison with the more rigorous but more expensive approaches.

II. IMPROVEMENTS TO ATOM-IN-JELLIUM CALCULATIONS

The original computer program implementing the atom-in-jellium calculation, INFERNO [13], suffered from some numerical problems in convergence and accuracy, beyond the limitations inherent in the atom-in-jellium model. For example, INFERNO experienced convergence problems including failure to complete calculations at temperatures below 0.1–1 eV. To address these problems, a revised program, PURGATORIO, was written [19]. PURGATORIO did not however include the ion-thermal calculation. With the help of diagnostics from a variety of FORTRAN compilers available on different computers, some errors were corrected in INFERNO, including functions returning incorrect values under some circumstances and machine-dependent problems arising from the alignment of different types of variables in common blocks. The resulting, modified program has been used periodically to calculate sets of states to help plan HED experiments [20].

INFERNO is typically used to run a sequence of calculations, and its performance on a calculation depends partly on variables set during the previous calculation. The program was found to perform best when used to calculate states along an isochore, starting at the highest temperature of interest.

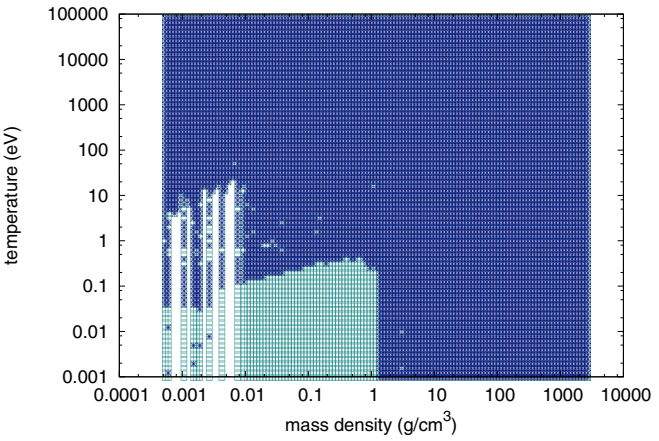

FIG. 1. Atom-in-jellium states calculated for Al. Dark blue: electron and ion calculations both completed. Light blue: ion calculation failed, indicating noninteracting atoms.

Using the modified version of INFERNO, and calculating down isochores in this way, atom-in-jellium computations were attempted over a range and density of states suitable for a general-purpose EOS: mass density ρ from 10^{-4} to $10^3\rho_0$ with 20 points per decade, and temperature T from 10^{-3} to 10^5 eV with ten points per decade. The electronic wave functions were found to be computed reliably down to 10 K or less for densities corresponding to condensed matter, and to 100 K or less for densities down to 0.1% of the ambient solid. At lower densities, calculations were completed successfully only for temperatures of several eV or more. Calculations of the ion oscillations tended to fail for densities below 10% of ambient and temperatures below ∼1 eV, where the electrons were localized on each atom and an Einstein frequency could not be determined. The ion-thermal calculation was found to fail or converge inaccurately for a small fraction of states with no discernible pattern to their distribution (Fig. 1).

The resulting fields were postprocessed to fill in isolated missing states and replace obvious numerical glitches, using polynomial interpolation from surrounding states. For each state, the Helmholtz free energy f was calculated, and then differentiated using a quadratic fit to the three closest states in ρ to determine the pressure $p(\rho, T)$ in tabular form. Similarly, quadratic fits in T were differentiated to find the specific entropy s and hence the specific internal energy $e(\rho, T)$ in tabular form. These tabulated functions comprise an EOS in SESAME or LEOS form.

Calculations were performed for a selection of elements desirable for interpreting HED experiments and for comparison with calculations performed using other techniques. In this paper, we show results for Be, Al, Si, Fe, and Mo. The first four are interesting to compare with recent PAMD results [16,17] as the closest but more sophisticated equivalent to the present method. Al, Fe, and Mo are standard materials for which considerable experimental and theoretical research has been reported. Al and Mo have been the subject of previous atom-in-jellium studies, but in a more limited way [13]. The computational cost of calculating a wide-ranging EOS increases much more quickly with atomic number for PIMC, QMD, and even PAMD, than for atom-in-jellium. Not enough

of the EOS has been tabulated to allow the construction of principal shock Hugoniot over a wide pressure range for Fe or Mo using these more rigorous techniques. We report our construction of wide range EOS for Fe and Mo using the atom-in-jellium approach, providing predictions which may be tested later when the more computationally intensive prescriptions can be applied, or experimental data may be available. It is also instructive to compare the predicted evolution of the effects of ionization of successive electron shells on the shock Hugoniot, with increasing atomic number.

For consistency with previous atom-in-jellium calculations, the exchange-correlation functional was the Hedin-Lundqvist form [21]. Calculations using Kohn-Sham [10] and Perdew-Zunger [22] functionals were found to make an insignificant difference to the EOS in the warm dense matter regime, compared with the inaccuracy of using the average-atom model instead of a three-dimensional treatment of the electron distribution. We would expect gradient-based or hybrid exchange-correlation treatments to make similarly little difference in this regime, in line with previously reported results such as [23]. A single set of solver parameters [24] was used for all calculations.

Because the atom-in-jellium model is a simplified representation of ion and electron distributions in three dimensions, there is ambiguity in performing some computations. The integrals over the continuum electronic states associated with an atom can be performed over the entire computational domain, or restricted to the inside of the cavity in the jellium. Thermodynamic quantities in the model can be defined as the difference between the calculation for a uniform electron gas with a given chemical potential, and the calculation for an atom inserted into a cavity in the uniform electron gas. The insertion may be performed at constant total volume or at constant volume of the uniform jellium, the difference being a slightly different electron density at the boundary. Calculations were performed with three alternative combinations of these choices [13,25]:

A: integrals over continuum states taken over the volume of the cavity, cavity inserted into the jellium at constant total volume (compressing the jellium as the cavity is added);

B: integrals taken over the cavity, cavity inserted into the jellium at constant jellium volume (expanding the total volume by the volume of the cavity);

T: integrals taken over the whole domain, cavity inserted into the jellium at constant total volume.

Results from the alternative treatments can be regarded as reflecting systematic uncertainties in the atom-in-jellium EOS. Typically, the models produce significantly different EOS at low temperatures, but they converge at temperatures above 1 eV or so. Anecdotally, model A has generally been found to be least inaccurate at low temperatures, but this is not the case for all elements.

The simplest test of a theoretical EOS is how well it reproduces the observed standard temperature and pressure (STP) state [26]. Multiatom electronic structure calculations based on variants of the local density approximation typically achieve accuracies of ∼1% in lattice parameter, or a few gigapascals in pressure. Atom-in-jellium results are significantly less accurate, as expected (Table I). All calculations used exactly the same solver parameters. The atom-in-jellium model cannot distinguish solid phases or between magnetic and nonmagnetic structures.

TABLE I. Pressure calculated at observed STP mass density ρ_0 and temperature, for each atom-in-jellium model.

Element	ρ_0 (g/cm^3)	A (GPa)	B (GPa)	T (GPa)
Be	1.85	6.2	−1.2	11.7
Al	2.70	3.4	−1.5	5.6
Si	2.33	−178.5	−261.0	−253.0
Fe	7.86	−59.1	−93.1	−70.2
Mo	10.28	−37.5	−60.6	−50.1

At STP, Al is close packed and Be is near close packed (hexagonal structure with c/a less than for ideal hexagonal close packing), and the discrepancy for both elements is relatively small at a few gigapascals. Fe and Mo are both body-centered cubic, the former stabilized by magnetic ordering; the discrepancy is a few tens of gigapascals, smaller for Mo. Si is diamond cubic, stabilized by directional covalent-type bonding which is not captured at all by the atom-in-jellium model, and has a discrepancy of around 200 GPa. The discrepancy thus reflects the relative unsuitability of using a spherical atom-in-jellium treatment for an element exhibiting a given degree of directional bonding, though the performance for Be was unexpectedly accurate. These discrepancies are a reflection of how far from ambient a material may have to be in order for the atom-in-jellium calculation to be useful.

III. GENERALIZED DEBYE MODEL

In the ion thermal model developed for use with atom-in-jellium calculations [18], perturbation theory was used to calculate the Hellmann-Feynman force on the ion when displaced from the center of the cavity in the jellium. Given the force constant $k = -\partial f/\partial r$, the Einstein vibration frequency $\nu_E = \sqrt{k/m_a}$ was determined, where m_a is the atomic mass, and hence the Einstein temperature $\theta_E = \hbar\nu_E/k_B$. The Debye temperature θ_D was inferred from θ_E, either by equating the ion-thermal energy or the mean square displacement.

The ion displacement calculation can be performed independently at every (ρ, T) state, and therefore θ_E and θ_D, unusually, depend on temperature as well as mass density. In contrast, in the Debye model of heat capacity as is commonly applied to condensed matter, θ_D is assumed to be a function of ρ only. In practice as calculated using the atom-in-jellium model, these characteristic temperatures vary greatly over the wide temperature ranges applicable to warm dense matter experiments (Fig. 2). Interpreting the atom-in-jellium results, the electronic states vary as the atom is heated, and the effect is to increase the restoring force against displacement of the nucleus from equilibrium. For all elements studied so far, θ_D increased much more slowly than T itself. The free energy in the Debye model is calculated independently for each (ρ, T) state, so there is no problem in using θ_D varying with T as well as ρ in the usual free energy calculation (below) without further modification.

The temperature dependence of θ_D in these calculations arises solely from thermal excitation of the electrons.

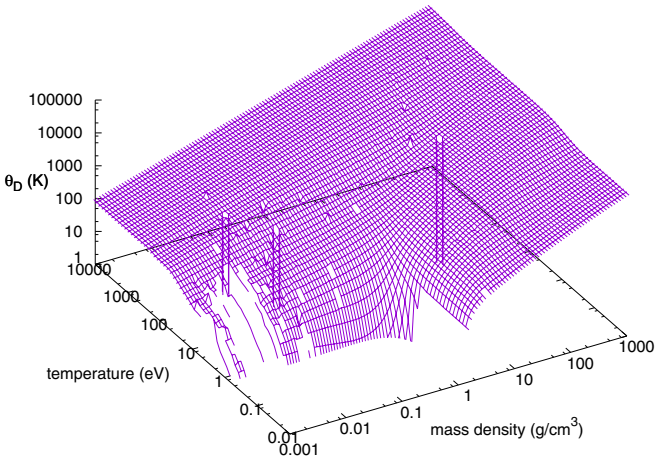

FIG. 2. Debye temperature calculated for Al.

This behavior is distinct from temperature dependence related to anharmonicity in the effective interatomic potential, causing interactions between phonons in the crystal lattice [27].

Another interesting aspect of the θ_D calculations is that they predict an abrupt transition from matter in tension, where the mass density is lower than at zero pressure but there is still a restoring force on the displaced nucleus, to instability with respect to perturbations as the electrons localize on the atom and effectively cease to interact with neighboring atoms as represented by the jellium. As the temperature is raised at constant density, this instability eventually disappears even before ionization takes place, as electrons are promoted to higher-energy bound states with larger tails at increased radius, extending more significantly into the jellium. The boundary between the two behaviors provides an estimate of the high-density side of the liquid-vapor region, up to the critical point. The atom-in-jellium calculation did not include any estimate of cluster formation in small groups of atoms, and would not be expected to give a prediction of the low-density side of the liquid-vapor region. The displaced-nucleus calculation in effect gives the polarizability of the jellium, and so is closely related to the van der Waals forces thought to govern the location of the critical point [28]. It is difficult to extract a precise prediction of the critical point from the atom-in-jellium calculations, as they are relatively flat in ρ and predict a gradual variation from $\theta_D = 0$ (a noisy contour) to several kelvin over several thousand kelvin, but the results are broadly consistent with other estimates, except for the critical temperature of Mo (Table II).

Given $\theta_D(\rho, T)$, the ion-thermal free energy can be calculated from

$$f_i = k_B T \left[3 \ln(1 - e^{-\theta_D/T}) + \frac{9\theta_D}{8T} - D_3(\theta_D/T) \right], \quad (1)$$

where $\frac{9}{8} k_B \theta_D$ is the zero-point energy and D_3 is the Debye integral,

$$D_3(x) \equiv \frac{3}{x^3} \int_0^x \frac{x^3\, dx}{e^x - 1}. \quad (2)$$

In practice, it was sometimes difficult to correct all the states affected by numerical noise from $\theta_D(\rho, T)$. However, the precise value of θ_D is only important when the temperature is similar to the Debye temperature. When $T \ll \theta_D$, the ionic heat capacity approaches zero, and when $T \gg \theta_D$, the ionic modes are all saturated. Thus, in most cases, an adequate representation of the generalized Debye heat capacity was found by using $\theta_D(\rho) : \theta_D(\rho, T) = T$, i.e., for any ρ, the value of θ_D chosen was that where it became equal to the temperature. It was much easier to remove or adjust noisy states from this one-dimensional tabulation (Fig. 3).

At sufficiently high temperatures, the ions become free and their specific heat capacity falls from $3k_B$ to $3k_B/2$ per atom, where k_B is the Boltzmann constant. The Debye free energy was modified to account for this freedom using a variant of the Cowan model [34].

IV. STATES AT ELEVATED MASS DENSITY AND TEMPERATURE

The atom-in-jellium and PAMD methods were originally developed to calculate states under warm dense matter conditions of compression and heating into the plasma regime, which is also most tractable for PIMC and QMD. All electronic structure methods naturally calculate states at a chosen mass density and temperature, so comparisons of specific states or loci where one is held constant, i.e., isotherms and isochores, are the most direct as they involve the specific, local results from each method. In contrast, shock Hugoniots involve the initial state as well as the shock state, which is generally less accurate for the atom-in-jellium model, and isentropes involve either the initial state to establish the entropy or an integration from the initial state to calculate the work of compression. Hugoniot calculations were made using the observed STP mass density, taking the atom-in-jellium calculation of specific internal energy (dominated by

TABLE II. Critical point.

	This work		Literature		
Element	ρ_c(g/cm^3)	T_c (K)	ρ_c(g/cm^3)	T_c (K)	References
Be	0.20–0.25	5000–6500	0.25–0.55	5300–9200	[29]
Al	0.43–0.70	4200–5500	0.69	7100–8600	[28]
Si	0.65–1.00	7300–7500		5200	[30]
Fe	1.00–2.00	5900–7800	1.33–2.03	6750–9340	[28,31]
Mo	0.86–1.31	6100–7100	1.7–3.7	8000–17 000	[28,32]

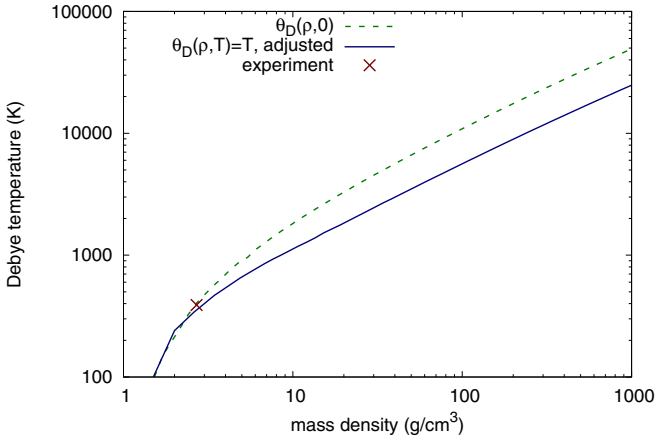

FIG. 3. Variation of Debye temperature with compression for Al, calculated with atom-in-jellium perturbation theory, compared with experimental value [33].

the binding energy of the inner electrons, which is likely to be accurate and far greater than the discrepancy in the outer electrons causing the pressure discrepancy), but setting the starting pressure to zero if the atom-in-jellium EOS has a negative value, which is a standard treatment for porous materials.

A. Beryllium

Atom-in-jellium states were extracted from the EOS along the 10-g/cm^3 isochore and 10-eV isotherm, which represent states relevant to ablators used for inertial confinement fusion experiments. The atom-in-jellium results were generally as close or closer to QMD results, compared with PAMD or previous average-atom Kohn-Sham results [17] (Figs. 4 and 5).

The shock Hugoniot from the atom-in-jellium EOS passed closely through published shock data up to 3.5 g/cm^3 [35,36], lay below the nuclear impedance match data of Nellis *et al.* [37], and passed within the larger error bars of nuclear

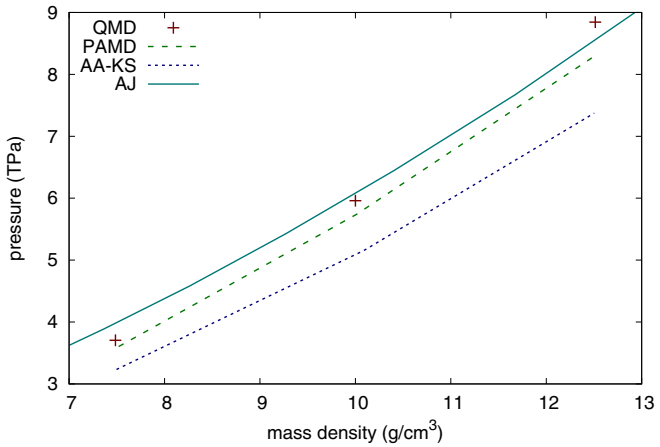

FIG. 4. Comparison of states calculated for Be along the 10-eV isotherm. AJ: atom-in-jellium (present work); QMD, PAMD, and average-atom Kohn-Sham (AA-KS) [17].

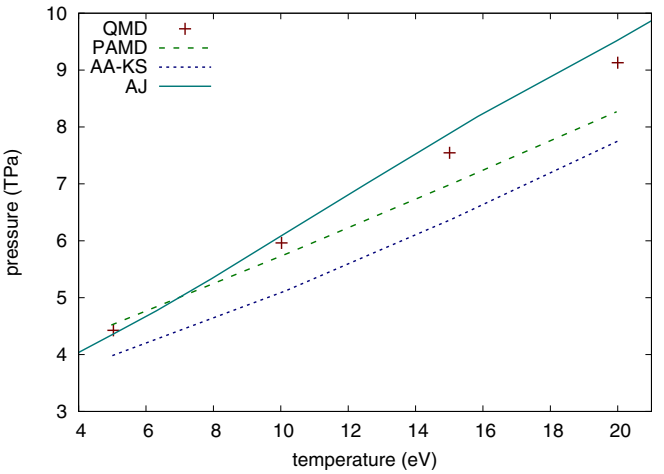

FIG. 5. Comparison of states calculated for Be along the 10 g/cm^3 isochore. AJ: atom-in-jellium (present work); QMD, PAMD, and average-atom Kohn-Sham (AA-KS) [17].

impedance match and laser-radiography data at higher pressures [38,39]. Previous EOS [2,40] were constructed using a straight-line fit to shock speed-particle speed data, TF theory for the electrons at higher pressure, and different prescriptions for the ion-thermal energy. The variation between the TF Hugoniots indicates the sensitivity to relatively subtle differences in the construction of EOS nominally all based on the same TF theory. The peak compression along the Hugoniot, at around 50 TPa, and not constrained by existing experimental measurements, was ∼6% higher from the atom-in-jellium calculation than from the TF EOS. This is a significant difference, and is even larger in terms of pressure, and should be observable in high pressure shock experiments such as are becoming possible on high-energy pulsed lasers [41]. At even higher pressures, the different atom-in-jellium models diverged (Fig. 6).

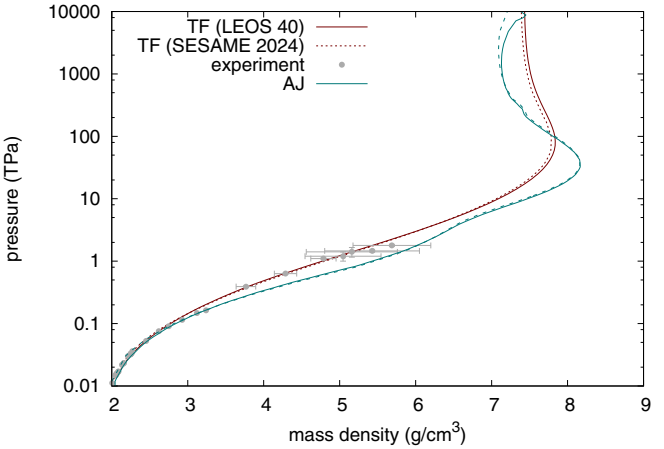

FIG. 6. Shock Hugoniot for Be, showing comparison between atom-in-jellium (AJ, present work) EOS constructed using models A and T (dashed, coincident) and B (solid), and TF EOS constructed with slightly different ion-thermal treatments [2,40], with experimental measurements [35–39].

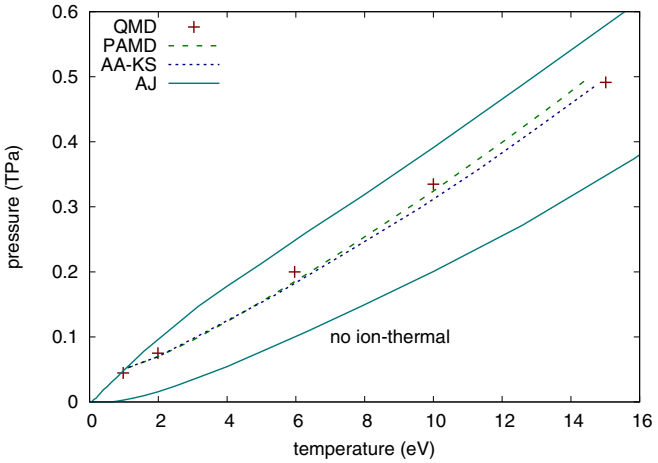

FIG. 7. States calculated for Al along the 2.7-g/cm^3 isochore. Atom-in-jellium (AJ, present work) is shown with and without the ion-thermal contribution, and compared with QMD, PAMD, and average-atom Kohn-Sham (AA-KS) [17].

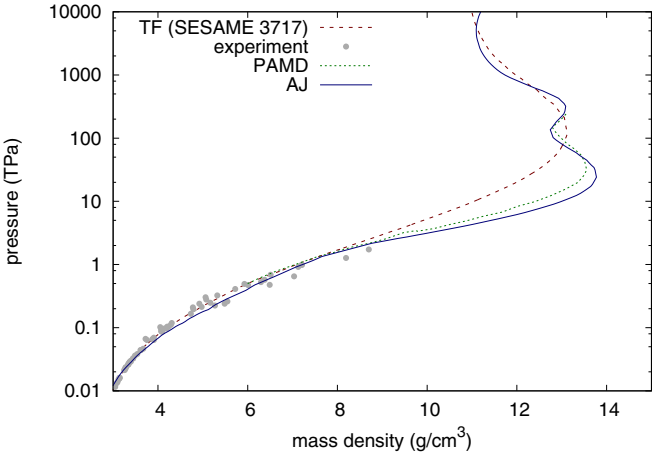

FIG. 8. Shock Hugoniot for Al, showing comparison between atom-in-jellium EOS (AJ, present work), an example TF-based EOS [46], and PAMD results [17], with experimental measurements [35,36,44].

EOS for Be have been constructed previously using atom-in-jellium calculations for the electron-thermal excitations only. One of these EOS included detailed DFT and QMD treatments of the solid and liquid phases [42]; the cold curve and ion-thermal treatment for the other EOS [43] were not reported. The Hugoniot from our completely atom-in-jellium results was consistent with the former EOS, in the liquid and plasma regime, but differed from the latter.

B. Aluminum

Atom-in-jellium states were extracted from the EOS along the 2.7-g/cm^3 isochore. The atom-in-jellium results were significantly stiffer than previously reported QMD, PAMD, and average-atom Kohn-Sham results at these relatively low pressures [17] (Fig. 7). The difference stands out in this comparison because the range is narrower than for other materials below, and the magnitude of the difference is similar at $o(0.1)$ TPa. Comparing the total pressure with the contributions from the electrons alone, the difference could be caused by an overprediction of the ion-thermal pressure by a few tens of percent. The difference could be reconciled by a faster decrease in ion-thermal heat capacity as the kinetic energy of the ions approaches the binding energy, and thus the attractive potential between the ions becomes saturated, beyond the Cowan modification to the Debye model. This will be the subject of a future study.

The shock Hugoniot for Al lay at significantly higher density than observed in the solid, but passed within the scatter in the data [35,36,44] for Al shocked above melting. The behavior closely followed PAMD and PIMC calculations [17,45] at higher pressures, exhibiting structure as bound electrons were ionized that departed significantly from a typical TF-based EOS [46] (Fig. 8).

C. Silicon

Atom-in-jellium states were extracted from the EOS along isochores from one to six times ρ_0. Despite the relatively large disagreement with the pressure at STP, the calculations reproduced previous PIMC and QMD results only slightly less well than PAMD [17] (Fig. 9). This result suggests that a relatively large inaccuracy in atom-in-jellium predictions in a solid around STP does not mean that the EOS will be inaccurate in the warm dense matter regime. Directional bonds from the outer electrons should disappear as the atoms become ionized. Directionality presumably becomes weaker in the liquid; even if present, it may have a negligible effect compared with the typical uncertainties in HED measurements.

The shock Hugoniot was very close to results from PIMC [47], which had a slightly lower peak compression than PAMD calculations [17]. All three shell structure techniques predicted features in the Hugoniot as bound electrons became ionized, differing substantially from TF predictions [2,48]. The latter is a combination of multi-ion density functional theory (DFT) calculations for Si in the diamond phase [49]

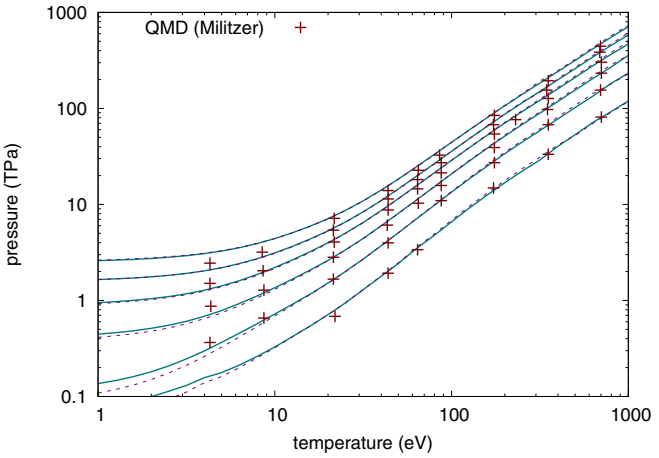

FIG. 9. States in Si along isochores at multiples of ρ_0 (lowest: $1 \times \rho_0$; highest: $6 \times \rho_0$). Atom-in-jellium calculations are shown for models A (dashed) and B (solid), compared with previous QMD calculations reported in [17].

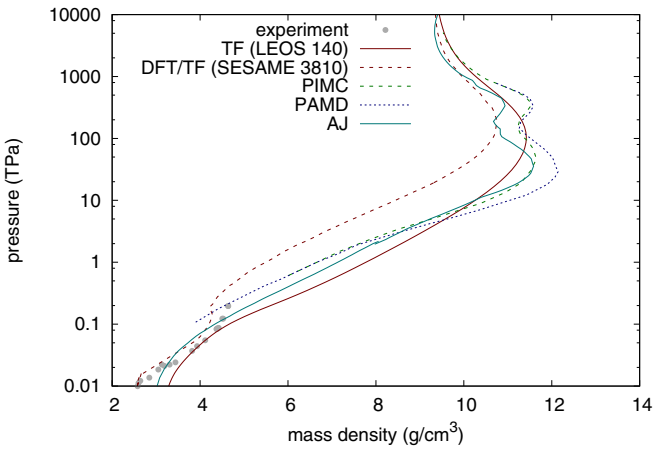

FIG. 10. Shock Hugoniot for Si, showing comparison between atom-in-jellium EOS (AJ, present work), two TF-based EOS [2,48], PIMC and PAMD calculations [17], and experimental measurements [44,50].

with an empirical piecewise linear representation of the principal Hugoniot based on that of Ge, to represent low-pressure shock data, linking to TF at high pressure and temperature. The resulting Hugoniot exhibits a jump of more than a factor of 2 in pressure near the limit in shock data [44,50] around 100 GPa, and lies well above the other EOS until above peak compression, suggesting that this EOS is probably very inaccurate above 100 GPa. The multi-ion calculations were subsequently extended to include the β-Sn phase of Si [51]. Calculations have since been performed for other phases, and a multiphase EOS valid to higher pressures is being constructed (Fig. 10).

D. Iron

QMD studies have been performed for Fe, to study the high-pressure melting curve for planetary physics [52,53], but less has been reported at higher temperatures relevant to warm dense matter and ionization features along the shock Hugoniot. Here we compare to the sparse QMD and PAMD results previously compared with PAMD calculations [17] (Table III). The atom-in-jellium results were similar to QMD where available and to PAMD, and the difference lay within the ion-thermal contribution to the EOS, again suggesting that the accuracy could be improved with a more sophisticated treatment of the reduction in ionic heat capacity from 3 to $\frac{3}{2}k_B$ per atom as the ions become free.

Previous wide-range EOS for Fe include several fitted to shock data where available and merging into TF theory at high temperature, such as LEOS 260 [2]. Iron exhibits solid-solid phase transitions with significant volume change, which are important for engineering applications involving elevated pressures and temperatures, such as armor. For that reason, considerable effort has been devoted to the development of multiphase EOS. One well-regarded and wide-range one [54] is a semiempirical multiphase construction including four solid phases and the liquid-vapor-plasma region. This EOS is notable here for using previous atom-in-jellium calculations, though for the electron-thermal contribution only.

Using the present atom-in-jellium prescription for the whole EOS, the calculated shock Hugoniot was too dense at pressures below 1 TPa, but then followed the (sparse) experimental data [35,36,44] within its scatter. The shell-structure EOS exhibited very similar modulation in compression around the peak, though different peak compressions, The TF and multiphase EOS were constructed using cold compression curves, combined with thermal excitation models for the ions and electrons. The cold compression curves were algebraic functions, Birch-Murnaghan in the case of the multiphase EOS [54], with a transition to TF at high density. It is striking that the TF and multiphase EOS predict similar Hugoniot shapes around peak compression, the difference being the additional modulation from the atom-in-jellium shell structure effect in the electron-thermal contribution to the multiphase EOS. Average-atom TF-based cold curves ignore the multicenter distribution of the nuclear potential, and the accuracy of almost all algebraic cold curves is at best unknown in extrapolation to higher densities than the fitting data, so it seems likely that the present, completely atom-in-jellium EOS gives a more accurate prediction of the peak compression. The difference amounts to a factor of 2–3 in pressure around 100 TPa, which should be observable in future HED experiments [55] (Fig. 11).

E. Molybdenum

Mo is interesting as a relatively high-Z element used as a high-pressure standard, for instance in impedance-matching measurements. It is also notable as being one of a small number of materials for which EOS were constructed consistently using atom-in-jellium calculations for the electron-thermal energy, combined with semirelativistic band structure calculations of the cold curve, to evaluate nuclear impedance-matching experiments [56]. Disappointingly, this EOS does not extend to a high enough temperature for the effects of shell structure to be evident.

Wide-ranging semiempirical EOS have been constructed using the standard prescription of an empirical fit to the shock

TABLE III. States in Fe. Previous results from [17].

Mass density (g/cm^3)	temperature (eV)	Pressure (TPa)					
		QMD	PAMD-KS	TFMD	PAMD-TF	This work	Electronic only
18.71	5	1.61	1.560		2.564	1.861	1.354
22.50	10	3.24	3.672	5.13	4.825	4.174	3.090
34.50	100		66.36	68.33	67.28	69.41	59.50
39.65	1000		1456.8	1476.5	1481.8	1497.6	1426.6

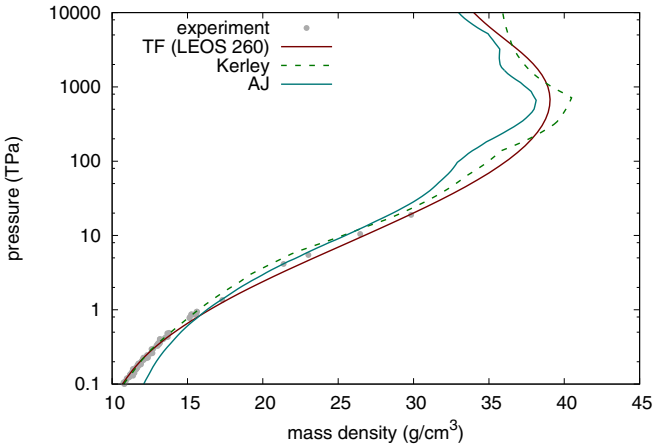

FIG. 11. Shock Hugoniot for Fe, showing comparison between atom-in-jellium EOS (AJ, present work), a semiempirical EOS incorporating shock data and TF theory [2], Kerley's semiempirical multiphase EOS which blends into TF theory for the cold curve and previous atom-in-jellium calculations for the electron-thermal contribution [54], and experimental measurements [35,36,44].

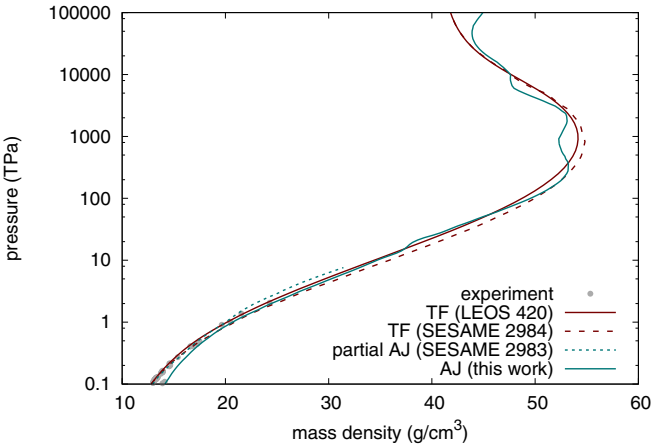

FIG. 12. Shock Hugoniot for Mo, showing comparison between atom-in-jellium EOS (AJ, present work), two semiempirical EOS using TF theory at high density and temperature [2,57], and experimental measurements [35,36,44]. Results from a previous EOS using atom-in-jellium calculations for the electron-thermal EOS only [56] are also shown, demonstrating that the temperature range of this EOS is insufficient to show shell structure effects.

Hugoniot and a transition to TF theory at high compression and temperatures [2,57]. Although constructed using very similar approaches, the TF-based EOS still differ significantly, particularly in the transition from the regime constrained by shock data to pressures of several times peak compression, where the TF contribution dominates equally in both. Neither PIMC nor PAMD simulations have been reported for Mo, and QMD simulations have not been reported at states high enough to explore ionization effects on the shock Hugoniot. The atom-in-jellium calculation of the complete, wide-ranging EOS was straightforward, and we include results here as a prediction for future comparison with more rigorous approaches. The present calculations had too high a density at low pressures, but passed within the scatter in published shock data [35,36,44] for pressures above 400 GPa. At higher pressures, the Hugoniot lay close to the TF EOS but exhibited several oscillations as successive electron shells were ionized. Although relatively modest when plotted over a wide pressure range, the effects of shell structure still amounted to localized pressure differences of up to a factor of 3 in comparison with TF, which should be observable with HED experimental platforms currently under development [55] (Fig. 12).

V. DISCUSSION

It may seem surprising that the atom-in-jellium technique published in 1979 [13] and extended to predict ion-thermal properties in 1990 [18] is still relevant. However, the standard method of constructing wide-range EOS is still based on empirical shock wave data in a framework of Mie-Grüneisen and classical Debye theory (1912) [58], with TF theory (1927) [3] at higher temperatures. Atom-in-jellium calculations have appeared relatively rarely in EOS libraries for a variety of reasons, including the higher computational cost than TF, the unproven predictions of shell structure effects which might be broadened by the effect of disorder on the ion positions, and the labor needed to adjust numerical parameters to achieve convergence or to correct for inadequacies by postprocessing individual calculations. Although the atom-in-jellium states implicitly include the cold contribution to the EOS, average-atom results are usually much less accurate around ambient density than multiatom electronic structure calculations, so the atom-in-jellium technique has generally been regarded as suitable for electron-thermal excitations only, as in the Fe and Mo EOS [54,56], and even then used rarely.

The updated atom-in-jellium program PURGATORIO is regarded as state of the art for calculating the electron-thermal contribution in wide-range EOS, and the predictions of shell effects on the Hugoniot are not universally accepted. PURGATORIO does not currently include an ion-thermal calculation; this contribution is added to the EOS using a simpler Debye-based model. Truly general-purpose EOS based on atom-in-jellium calculations are not yet widely available because of the extra complexity involved in combining them with a more accurate treatment of the solid state, which we have not attempted in the work reported here.

It is only recently, with the advent of the more rigorous theoretical techniques, that the shell structure predictions have been repeated independently, and over relatively narrow regions of state space. The LiF EOS whose recent comparisons with PIMC prompted the observation that shell-structure effects are supported by multiatom calculations [12] is a mixture of two elemental EOS, each constructed using PURGATORIO calculations of the electron-thermal energy, rather than a direct cross check without mixing. Although PIMC is expected to be accurate, it is so computationally expensive that its precision has been demonstrated only indirectly, by comparison with QMD simulations which can themselves be compared with shock, isothermal compression, or ambient data. The magnitude of the shell structure effects predicted is only modest compared with the spacing between states calculated with PIMC, so the detailed shape may depend partly on the method of interpolation between simulations.

Clear experimental evidence of the effects of shell structure is still lacking, though recent developments in converging shock techniques [41,55,59,60] mean that direct experimental comparisons may be possible.

A corollary is that EOS construction should proceed via a spectrum of computational tools, ranging from those capable of spanning a wide range of state space with as much rigor as is practical, complemented by a hierarchy of techniques of increasing rigor and computational cost to validate the EOS or highlight where corrections are needed. As computational resources and the sophistication of theoretical techniques increase, the overall accuracy and rigor of EOS should steadily improve. Guided by QMD and PIMC in the regimes where they are tractable, atom-in-jellium calculations are feasible for use now, and appear necessary to capture expected properties, for the construction of wide-ranging EOS for elemental plasmas. For mixed species, atom-in-jellium results must either be mixed using *ad hoc* models, or run with an averaged Z, which is physically dubious because the EOS of each component is highly nonlinear in Z; rigorous mixed-species plasma calculations are currently only possible using QMD and PIMC.

The calculation of $\theta_D(\rho, T)$ is an interesting generalization of the Debye model for ion-thermal energy, offering a wider range of validity than Mie-Grüneisen EOS constructed with $\theta_D(\rho)$. The related observation that a structure like the vapor dome appears in atom-in-jellium calculations was unexpected, and provides a different explanation for the physics behind the liquid-vapor region, although the EOS calculations themselves do not give a precise calculation of the critical point.

Considering shock Hugoniot curves, we showed various comparisons with EOS constructed using the present, fully atom-in-jellium approach, and other EOS. The comparisons included semiempirical EOS which were constrained by data, usually from shock experiments, blended into TF or TFD calculations for higher compressions and temperatures. We also showed a comparison with an example wide-range multiphysics EOS incorporating multiatom DFT and again blended into TF-type calculations outside the range of the DFT treatment [1]. Hugoniots vary even from EOS constructed using similar treatments by a single researcher on different occasions, as well as between different researchers and, even more so, between different groups using different computer programs. Hugoniots may vary even in the range of identical sets of constraining data, as different interpolating functions may be used and subsets of the data may be weighted differently when constructing the EOS. The Hugoniots vary even more markedly between these approaches and our fully atom-in-jellium calculations.

The deviation between different TF EOS became insignificant for shock pressures exceeding a few times the level needed to induce peak compression, because TF-like calculations themselves are relatively standard and equivalent, and in this regime the TF contribution dominates over differences in the treatment of the cold compression curve and the ion-thermal excitations. An exception may be for low-Z materials if the ion-thermal treatment is particularly crude, when the extra contribution of $\frac{3}{2}k_B$ per atom to the heat capacity from the potential modes of the ions may still be evident. The behavior of the EOS depends on the strategy chosen to switch between different physical approaches in different regimes of state space, which is not constrained well on physical grounds, and so is particularly prone to variations between different attempts at constructing a wide-range EOS for a given substance. These issues motivate the development of more rigorous theoretical techniques, but also of computationally efficient techniques enabling state space to be explored more widely and densely than with the most rigorous technique available at any juncture.

The atom-in-jellium model was developed precisely to extend the validity of TFD techniques toward ambient conditions, by capturing the physics of compressed and heated atoms more accurately [13]. Atom-in-jellium calculations should not be expected to be as accurate as PIMC, QMD, or PAMD calculations, but our results show that they are likely to be adequate for matter in the fluid and dense plasma regime, though not sufficiently accurate for solid elements near zero pressure. The more sophisticated techniques have better physical fidelity in their treatment of ionic motion as the ions transition from being bound, with fully populated vibrational modes and a heat capacity of $3k_B$ per atom, to an unbound state with a heat capacity from the kinetic modes only, and so falling to $\frac{3}{2}k_B$ per atom. This is, however, an area with potential for improvements to be made to atom-in-jellium calculations [61].

VI. CONCLUSIONS

Equations of state were constructed for five example elements, using atom-in-jellium calculations for the ion-thermal as well as electronic free energy. The elements chosen are all solids at STP, but spanned low to mid Z, and a range of types of electronic structure. The calculations were efficient enough to allow a wide-ranging EOS to be produced in a few CPU hours, and covering compressions and temperatures typical of general-purpose libraries such as SESAME and LEOS. Postprocessing is needed as a palliative for numerical noise and failed calculations in cool, expanded states.

The calculated states exhibit localization of the electrons at low temperatures in expansion, and suggest an atomistic interpretation of the critical point and boundary of the vapor region as the locus where atoms' respective electrons start to interact.

The atom-in-jellium EOS were generally inaccurate for states around STP, particularly for non-close-packed and covalently bonded structures, but became much more accurate at relatively modest temperatures or compressions, generally on heating beyond melt. For states representative of warm dense matter, the atom-in-jellium calculations agreed well with PAMD calculations, and gave a similar agreement with PIMC calculations. PIMC, QMD, and PAMD calculations were more sparse or absent for the higher-Z elements, but we made fully atom-in-jellium predictions of the principal shock Hugoniots for future comparison.

Semiempirical or multiphysics EOS constrained by shock data or multiatom DFT at low temperatures, and blended into TF-type calculations at higher temperatures, were shown to vary significantly at shock pressures from the top of the constraining data to pressures a few times higher than that corresponding to peak compression. Fully atom-in-jellium

calculations are likely to be more accurate in this regime as they capture more of the physics of the compressed, heated atoms, though PIMC, QMD, and PAMD calculations are likely to be more reliably accurate as the ion-thermal energy transitions from fully populated vibrational modes to unbound motion. There is scope for further improvement of the treatment of this regime in atom-in-jellium calculations.

Shock Hugoniots reproduced the locus of experimental data for pressures above a few hundred gigapascals, and (like PAMD and PIMC) exhibited structure as bound electrons were excited. These structures gave Hugoniots that were significantly different from TF-based EOS, though at higher Z the shell structure techniques tended toward the TF locus though still with significant deviations. Like PAMD, the atom-in-jellium calculations gave a slightly different peak Hugoniot compression. The deviations from EOS based on TF theory amount to tens to hundreds of percent in pressure, and several to ∼20% in mass density, for shock pressures of a few to ∼100 TPa. This differences should be observable using experimental techniques under development in HED facilities.

ACKNOWLEDGMENTS

B. Militzer (University of California, Berkeley) kindly provided numerical values from PIMC calculations for comparison. C. Starrett and C. Greeff (Los Alamos National Laboratory) gave extensive input and comments on the manuscript. This work was performed under the auspices of the U.S. Department of Energy under Contract No. DE-AC52-07NA27344.

[1] S. P. Lyon and J. D. Johnson, Los Alamos National Laboratory Report No. LA-UR-92-3407, 1992.
[2] D. A. Young and E. M. Corey, J. Appl. Phys. **78**, 3748 (1995).
[3] L. H. Thomas, Proc. Cambridge Philos. Soc. **23**, 542 (1927); E. Fermi, Rendiconti Lincei **6**, 602 (1927).
[4] P. A. M. Dirac, Math. Proc. Cambridge Philos. Soc. **26**, 376 (1928).
[5] R. W. Zwanzig, J. Chem. Phys. **22**, 1420 (1954); B. J. Alder and C. E. Hecht, *ibid.* **50**, 2032 (1969).
[6] E. L. Pollock and D. M. Ceperley, Phys. Rev. B **30**, 2555 (1984).
[7] L. Collins, I. Kwon, J. Kress, N. Troullier, and D. Lynch, Phys. Rev. E **52**, 6202 (1995).
[8] D. M. Ceperley, J. Stat. Phys. **63**, 1237 (1991).
[9] P. Hohenberg and W. Kohn, Phys. Rev. **136**, B864 (1964).
[10] W. Kohn and L. J. Sham, Phys. Rev. **140**, A1133 (1965).
[11] L. X. Benedict, K. P. Driver, S. Hamel, B. Militzer, T. Qi, A. A. Correa, A. Saul, and E. Schwegler, Phys. Rev. B **89**, 224109 (2014).
[12] K. P. Driver and B. Militzer, Phys. Rev. E **95**, 043205 (2017).
[13] D. A. Liberman, Phys. Rev. B **20**, 4981 (1979).
[14] B. F. Rozsnyai, J. R. Albritton, D. A. Young, V. N. Sonnad, and D. A. Liberman, Phys. Lett. A **291**, 226 (2001).
[15] G. Zérah, J. Clérouin, and E. L. Pollock, Phys. Rev. Lett. **69**, 446 (1992).
[16] C. E. Starrett, J. Daligault, and D. Saumon, Phys. Rev. E **91**, 013104 (2015).
[17] C. E. Starrett and D. Saumon, Phys. Rev. E **93**, 063206 (2016).
[18] D. A. Liberman and B. I. Bennett, Phys. Rev. B **42**, 2475 (1990).
[19] B. Wilson, V. Sonnad, P. Sterne, and W. Isaacs, J. Quant. Spectrosc. Radiat. Transfer **99**, 658 (2006).
[20] D. C. Swift (unpublished).
[21] L. Hedin and B. I. Lundqvist, J. Phys. C: Solid State Phys. **4**, 2064 (1971).
[22] J. P. Perdew and A. Zunger, Phys. Rev. B. **23**, 5048 (1981).
[23] T. Sjostrom, S. Crockett, and S. Rudin, Phys. Rev. B **94**, 144101 (2016).
[24] B. I. Bennett (Los Alamos National Laboratory) (unpublished).
[25] B. I. Bennett and D. A. Liberman, Los Alamos National Laboratory Report No. LA-10309-M, 1985.
[26] In this work, the National Institute of Standards and Technology (NIST) definition of standard temperature and pressure (STP) was used: 293 K and 1.013×10^{-4}GPa. Compared with the deviation of the theoretical EOS from each other and from STP up to HED states, the difference from using the International Union of Pure and Applied Chemistry definition of STP (or of including more decimal places in the NIST definition) is negligible.
[27] For instance, M. P. Tosi and F. G. Fumi, Phys. Rev. **131**, 1458 (1963); X.-X. Ren, W. Kang, Z.-F. Cheng, and R.-L. Zheng, Chin. Phys. Lett. **33**, 126501 (2016).
[28] D. A. Young and B. J. Alder, Phys. Rev. A **3**, 364 (1971).
[29] E. M. Apfelbaum, J. Phys. Chem. B **116**, 14660 (2012).
[30] Website of EL-CAT Inc., https://www.el-cat.com/silicon-properties.htm retrieved on 9/21/2018.
[31] M. Beutl, G. Pottlacher, and H. Jäger, Int. J. Thermophysics **15**, 1323 (1994).
[32] D. V. Minakov and P. R. Levashov, J. Phys.: Conf. Ser. **946**, 012093 (2018).
[33] C. Y. Ho, R. W. Powell, and P. E. Liley, J. Phys. Chem. Ref. Data **3**, 1 (1974).
[34] C. W. Cranfill and R. More, Los Alamos Scientific Laboratory Report No. LA-7313-MS (1978); R. M. More, K. H. Warren, D. A. Young, and G. B. Zimmerman, Phys. Fluids **31**, 3059 (1988).
[35] *LASL Shock Hugoniot Data*, edited by S. P. Marsh (University of California, Berkeley, 1980).
[36] M. van Thiel, Compendium of Shock Wave Data, Lawrence Livermore National Laboratory Report No. UCRL-50108, 1966.
[37] W. J. Nellis, J. A. Moriarty, A. C. Mitchell, and N. C. Holmes, J. Appl. Phys. **82**, 2225 (1997).
[38] C. E. Ragan III, Phys. Rev. A **25**, 3360 (1982).
[39] R. Cauble, T. S. Perry, D. R. Bach, K. S. Budil, B. A. Hammel, G. W. Collins, D. M. Gold, J. Dunn, P. Celliers, L. B. Da Silva, M. E. Foord, R. J. Wallace, R. E. Stewart, and N. C. Woolsey, Phys. Rev. Lett. **80**, 1248 (1998).
[40] J. D. Johnson (Los Alamos National Laboratory), unpublished documentation for SESAME EOS 2024, 1992.
[41] A. L. Kritcher, T. Doeppner, D. Swift, J. Hawreliak, J. Nilsen, J. Hammer, B. Bachmann, G. Collins, O. Landen, C. Keane, S. Glenzer, S. Rothman, D. Chapman, D. Kraus, and R. W. Falcone, J. Phys.: Conf. Ser. **688**, 012055 (2016).

[42] L. X. Benedict, T. Ogitsu, A. Trave, C. J. Wu, P. A. Sterne, and E. Schwegler, Phys. Rev. B **79**, 064106 (2009).
[43] Y. H. Ding and S. X. Hu, Phys. Plasmas **24**, 062702 (2017).
[44] R. F. Trunin, L. F. Gudarenko, M. V. Zhernokletov, and G. V. Simakov, *Experimental Data on Shock Compression and Adiabatic Expansion of Condensed Matter* (Russian Federal Nuclear Center, Sarov, 2001).
[45] K. P. Driver, F. Soubiran, and B. Militzer, Phys. Rev. E **97**, 063207 (2018).
[46] J. Barnes and S. Lyon, Documentation for SESAME EOS 3717, Los Alamos National Laboratory (1988).
[47] S.-X. Hu, B. Militzer, L. A. Collins, K. P. Driver, and J. D. Kress, Phys. Rev. B **94**, 094109 (2016).
[48] J. D. Johnson and S. Lyon, Documentation for SESAME EOS 3810, Los Alamos National Laboratory, 1997.
[49] D. C. Swift, U.K. Atomic Weapons Establishment Report No. AWE-HD01-R-9705, 1997.
[50] M. N. Pavlovskii, Sov. Phys.-Solid State **9**, 11 (1967).
[51] D. C. Swift, G. J. Ackland, A. A. Hauer, and G. A. Kyrala, Phys. Rev. B **64**, 214107 (2001).
[52] G. Morard, J. Bouchet, D. Valencia, S. Mazevet, and F. Guyot, High Energy Density Phys. **7**, 141 (2011).
[53] J. Bouchet, S. Mazevet, G. Morard, F. Guyot, and R. Musella, Phys. Rev. B **87**, 094102 (2013).
[54] G. I. Kerley, Sandia National Laboratories Report No. SAND93-0227, 1993.
[55] A. Jenei *et al.* (unpublished).
[56] K. Trainor, Documentation for SESAME EOS 2983, Los Alamos National Laboratory, 1983.
[57] J. D. Johnson and S. Lyon, Documentation for SESAME EOS 2984, Los Alamos National Laboratory, 1997.
[58] P. Debye, Ann. Phys. **344**, 789 (1912).
[59] D. C. Swift, A. L. Kritcher, J. A. Hawreliak, A. Lazicki, A. MacPhee, B. Bachmann, T. Döppner, J. Nilsen, G. W. Collins, S. Glenzer, S. D. Rothman, D. Kraus, and R. W. Falcone, Rev. Sci. Instrum. **89**, 053505 (2018).
[60] T. Döppner, D. C. Swift, A. L. Kritcher, B. Bachmann, G. W. Collins, D. A. Chapman, J. Hawreliak, D. Kraus, J. Nilsen, S. Rothman, L. X. Benedict, E. Dewald, D. E. Fratanduono, J. A. Gaffney, S. H. Glenzer, S. Hamel, O. L. Landen, H. J. Lee, S. LePape, T. Ma *et al.*, Phys. Rev. Lett. **121**, 025001 (2018).
[61] D. C. Swift, M. Bethkenhagen, A. A. Correa, T. Lockard, S. Hamel, L. X. Benedict, P. A. Sterne, and B. I. Bennett, arXiv:1905.08911 (2019).